

# Chapter I

## Magneto-optical study of Cr-doped CdTe quantum dots

In this chapter, we will study the photoluminescence of a II-VI quantum dot containing a single Chromium atom. We saw in the chap. ?? that the magnetic anisotropy of the spin lead to a zero magnetic field splitting of the 0,  $\pm 1$  and  $\pm 2$  states. In a neutral Cr-doped quantum dot, such an anisotropy is induced by the bi-axial strains in the plane of the dots. Probing optically the dot, it results that exchange interaction is enough to see the effect of the presence of a single Cr spin in the QD. Studying the magnetic-field dependence of the quantum dots photoluminescence, we will also show the influence of the symmetry on carrier-Cr spin coupling.

### I.1 Strained quantum dots containing an individual Cr atom

#### I.1.1 Energy structure of a Cr in a quantum dot

Using the procedure described in the chap. ??, we randomly incorporated Cr atom in CdTe/ZnTe quantum dots, adjusting the density of the Cr atoms to be roughly equal to the density of dots, in order to get QDs containing 0, 1 or a few Cr atoms. The photoluminescence (PL) of individual QDs, induced by optical excitation with a dye laser tuned on resonance with an excited state of the dots, is studied by optical micro-spectroscopy.

Low temperature ( $T=5K$ ) PL of the neutral exciton (X-Cr) of several QD doped with a single Cr are reported in Fig. I.1. Four emission lines are observed as shown in QD3, with the central peak being split in some QDs, such as QD1 and QD2 spectra. Scanning with an energy tunable laser, we saw that all the peaks

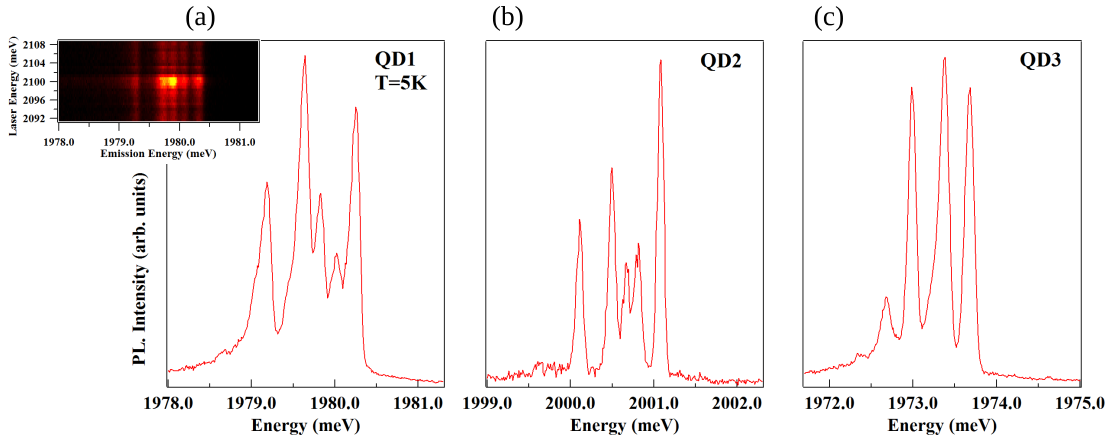


Figure I.1: (a) PL of QD1 X-Cr complex at low temperature (T=5K). Inset presents the PLE map of this QD, showing a sharp quasi-resonant state for an excitation at 2100 meV. (b) PL of QD2 X-Cr complex at low temperature. (c) PL of QD3 X-Cr complex at low temperature.

share a common quasi-resonant state, where all are at a maximum intensity, as highlighted in the inset of Fig. I.1(a). This is an indication that they originate from the same dot. Variations in the relative intensities of the peaks are observed in different dots. The lowest energy peak is shown as getting more intense when the splitting of the central peak get wider.

In a II-VI semiconductor, the orbital momentum of the Cr connects the spin of the atom to its local strain environment through the modification of the crystal field and the spin-orbit coupling. For biaxial strain in the (001) plane, the ground state of a Cr spin is split by a strain induced magnetic anisotropy term  $\mathcal{H}_{Cr,\varepsilon_{||}} = D_0 S_z^2$  (see chap. ??). It was deduced from electron paramagnetic resonance of bulk Cr-doped CdTe that  $D_0$  is positive for compressive biaxial strain [1]. In a self-assembled CdTe/ZnTe QD with large in-plane strain, the Cr spin energy levels are split with  $S_z=0$  at low energy (Fig. I.2). A value of  $D_0$  in the 1 meV range can be expected for a CdTe layer strained on a ZnTe substrate, as shown in chap. ??.

When an electron-hole (e-h) pair is injected in a Cr-doped QD, the bright excitons are split by the exchange interaction between the spins of Cr and carriers. In flat self-assembled QDs, the heavy-holes and light-holes are separated in energy by the biaxial strain and the confinement. In a first approximation, the ground state in such QD is a pure heavy-hole ( $J_z=\pm 3/2$ ) exciton and the exchange interaction with the Cr spin  $S$  is described by the spin Hamiltonian

$$\mathcal{H}_{c-Cr} = I_{eCr} \vec{S} \cdot \vec{\sigma} + I_{hCr} S_z J_z \quad (\text{I.1})$$

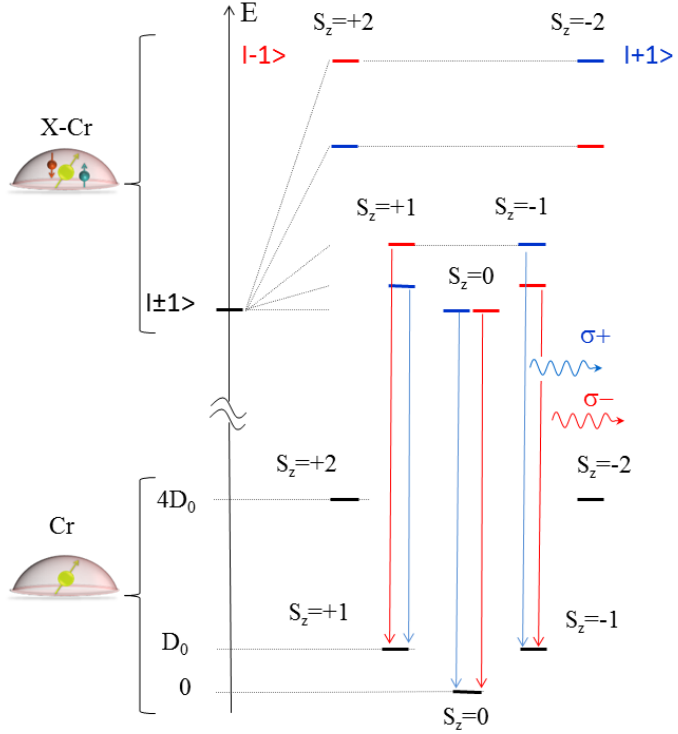


Figure I.2: Illustration of the energy levels of the ground state (Cr), the bright exciton states ( $|\pm 1\rangle$ ) coupled to the spin of a Cr (X-Cr) and dominant PL transitions ( $\sigma+$ ,  $\sigma-$ ). The states  $|S_z = \pm 2\rangle$  cannot be populated through thermalization, and thus the recombination channel are not shown on this schema.

with  $\vec{\sigma}$  the electron spin and  $J_z$  the hole spin operator.  $I_{eCr}$  and  $I_{hCr}$  are, respectively, the exchange integrals of the electron and the hole spins with the Cr spin. These exchange energies depend on the exchange constant of the  $3d$  electrons of the Cr with the carriers in CdTe and on the overlap of the Cr atom with the confined carriers. The exchange interaction of the Cr spin is ferromagnetic for both electron and hole spins in common II-VI semiconductors and a typical exchange constant 4 to 5 times larger for the holes than for the electrons is also expected in CdTe [2, 3].

For highly strained CdTe/ZnTe QDs with a weak hole confinement, the strain induced energy splitting of the Cr spin  $D_0 S_z^2$  is much larger than the exchange energy with the confined carriers ( $D_0 \gg |I_{hCr}| > |I_{eCr}|$ ). The exchange interaction with the exciton acts as an effective magnetic field which further splits the Cr spins states  $S_z = \pm 1$  and  $S_z = \pm 2$ . The resulting X-Cr energy levels are presented in Fig. I.2. The exciton recombination does not affect the Cr atom and its spin

is conserved during the optical transitions. Consequently, the large strain induced splitting of the Cr spin is not directly observed in the optical spectra. However, at low temperature, the Cr spin thermalize on the low energy states  $S_z=0$  and  $S_z=\pm 1$ . This leads to a PL dominated by three contributions: a central line corresponding to  $S_z=0$  and the two outer lines associated with  $S_z=\pm 1$  split by the exchange interaction with the carriers.

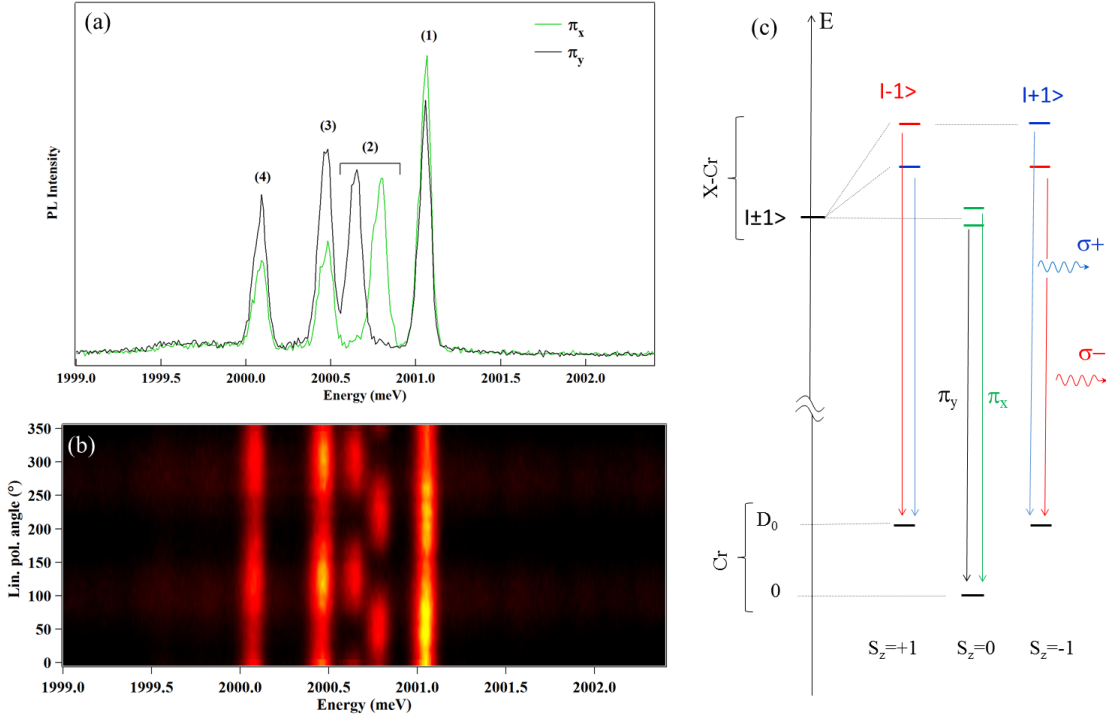


Figure I.3: (a) Low temperature ( $T=5\text{K}$ ) PL of QD2 recorded in circular polarization:  $\sigma+$  in blue and  $\sigma-$  in red. (b) Low temperature PL of QD2 recorded along two orthogonal directions. (c) Linear polarization PL intensity map of QD2. The  $0^\circ$  polarization angle corresponds to an emission polarized along the QD cleavage axis, either  $110$  or  $\bar{1}\bar{1}0$ . (d) Illustration of the energy levels of the ground state (Cr), the bright exciton states ( $| \pm 1 \rangle$ ) coupled to the spin of a Cr (X-Cr), showing the splitting of the central peak via the bright exciton coupling, and dominant PL transitions ( $\sigma+$  (blue),  $\sigma-$  (red) and  $\pi$  (green and black)).

Cr-doped quantum dots exhibit a linear polarization dependence, as presented in Fig. I.3. The central line ( $S_z=0$ ) is split and linearly polarized along two orthogonal directions. As in non-magnetic QDs, this results from a coupling of the two bright excitons  $|\pm 1\rangle$  by (i) the short range e-h exchange interaction in the presence

of valence band mixing and/or (ii) the long-range e-h exchange interaction in a QD with an in-plane shape anisotropy [4]. This anisotropic e-h exchange energy mixes the bright exciton associated with the same Cr spin state, inducing an extra splitting between them. The mixing is maximum for the central pair of bright excitons ( $S_z=0$ ) which are initially degenerated. The outer lines are also slightly linearly polarized but the influence of the e-h exchange interaction is attenuated by the initial splitting of the  $|\pm 1\rangle$  excitons induced by the exchange interaction with the Cr spin  $S_z=\pm 1$ .

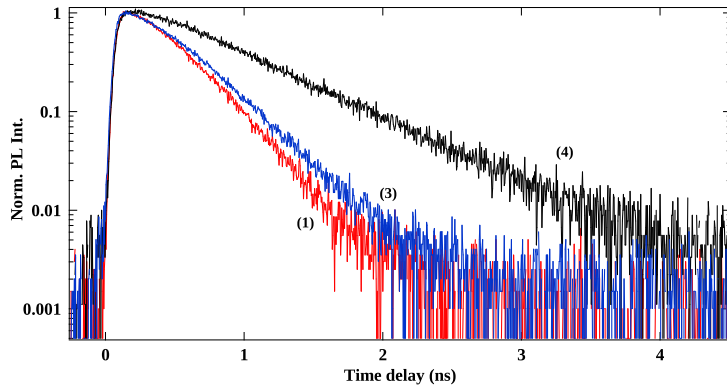


Figure I.4: Time resolved PL of QD2 taken on two exterior peaks, attributed to  $|S_z = +1\rangle$  and  $|S_z = -1\rangle$  (noted (1) and (3) in Fig. I.3(a)), and the lower energy one (noted (4)).

In order to identify the lower energy peak ((4) in Fig. I.3(a)), we took the time resolved photoluminescence of the emission peaks, presented in Fig. I.4. One can notice that the line (4) present a decay time about twice as long as the high energy peak. A long recombination time is one of the characteristics of a dark exciton emission [5]. Under normal circumstances, the recombination of such a state is non-radiative. However, it is possible to observe a dark exciton recombination emitting a photon in low symmetry quantum dot [6]. This hypothesis will be confirmed by the magneto-optical study of the dot presented in Fig. I.9 and I.11.

Since the absence of PL on  $|\pm 2\rangle$  is linked to their impossibility to be thermally populated, one could expect to see their emission at higher temperature. Fig. I.5 presents the dot PL at several temperatures. With the increase of the temperature, we observe a significant line broadening induced by the interaction with acoustic phonons. In order to keep a significant PL intensity and resolved PL lines, we limited our investigation to temperature below 50K. No contribution of the  $|S_z=\pm 2\rangle$  Cr spins states are observed in the emission of the exciton.



Figure I.5: Temperature evolution of QD2 PL, from  $T=5\text{K}$  to  $T=40\text{K}$ . The red shift and peak broadening are clearly visible. Even at  $40\text{K}$ ,  $|\text{S}_z = \pm 2\rangle$  states do not appear.

### I.1.2 Excited states of a Cr-doped QD

In order to study the different excited states presented by a QD doped with a single Cr atom, we took the PLE of QD2 starting close the dot. The dot spectra is presented in Fig. I.6(a) in both  $\sigma$  polarizations. The central peaks do not show dependency in circular polarization, which is coherent with their linear polarization dependency presented in Fig. I.3(a) and (b). The excitation laser is  $\sigma+$  polarized in order to control the spin of the injected exciton. The exterior peaks emission being in  $\sigma+$  polarization shows that there is no spin flip of the exciton before recombination.

Fig. I.6(b) presents the entire PLE of QD2 X-Cr complex. However, one can note several other excited states along the scan. In this section, we will discuss several of them.

The first remarkable feature of this scan is the really long luminescence of the acoustic phonon replica. As shown on the zoom in Fig. I.7(a), the probed peak

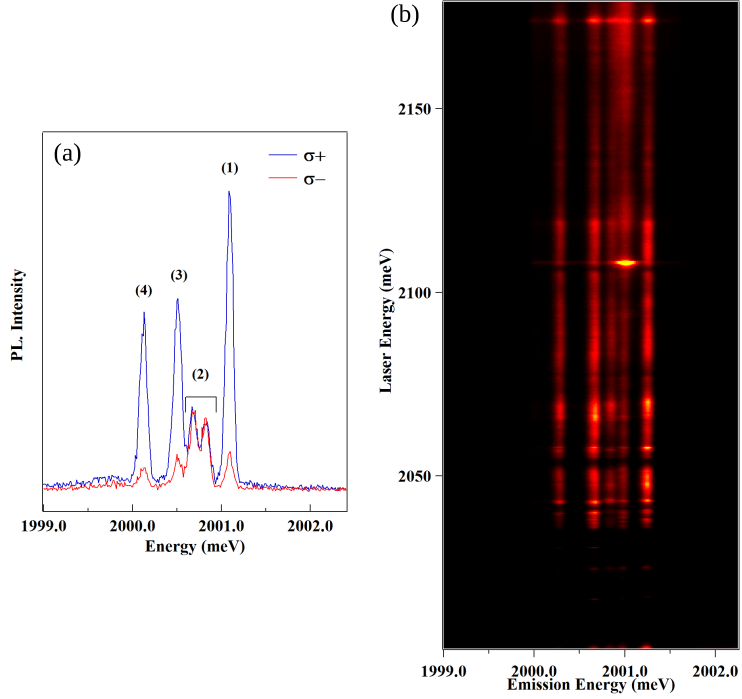


Figure I.6: (a) PL spectra of the exciton in QD2 (X-Cr) for co- and cross-circularly polarized excitation/detection [À VÉRFIER : taken on the 2175 meV quasi-resonant state]. (b) QD2 X-Cr PLE map in  $\sigma$ - polarization. Several excited states are identifiable and are discussed in Fig. I.7 and I.8.

continues to emit with an excitation several millielectronvolt above the excited state, remaining visible until 2004 meV. One can also see two sharp intensity diminutions in this emission. Mapping the intensity of this peak emission to the quantum dot spectrum (Fig. I.7(b)), it is evidenced that these diminutions occur when the laser is in resonance with a QD emission line. The absorption then preferentially occurs in this resonantly excited state than in the acoustic phonon band.

At higher excitation energy, several excited states appear. The lower energy one is around 2018.5 meV, zoomed in on Fig. I.8(d). On this excited state, each peak presents a slightly different resonant energy. One can see that the order of appearance of the two central peaks seems to be reversed compared to the external ones. This phenomenon was first observed on QDs in GaAs quantum well [7]. This indicates an inversion of the splitting due to electron-hole exchange interaction [4].

Another excited state can be saw at 2025 meV. This excited state occurs on a large energy band and can be linked back to an excitation to the optical phonon.

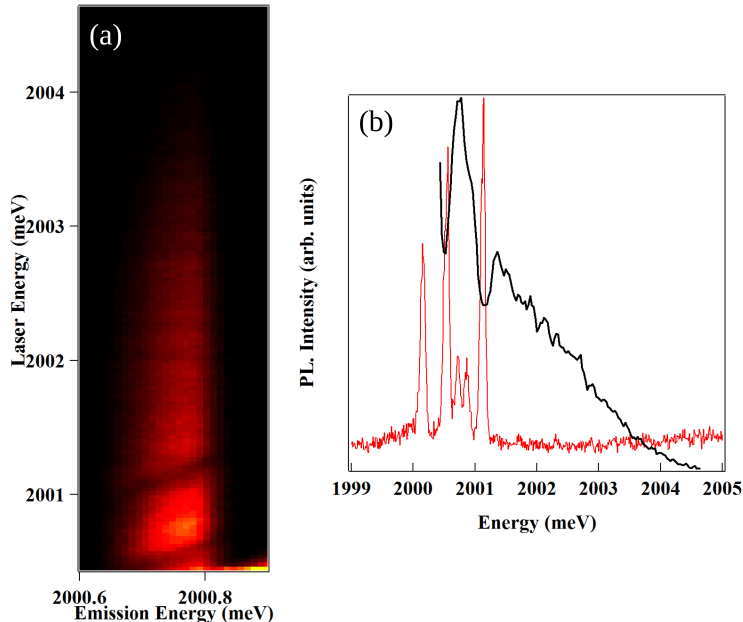


Figure I.7: (a) PLE scan of the lower energy peak, taken close to the QD emission energy, showing the phonon replica taken in  $\pi$  detection. The emission integrated intensity in function of the laser energy is plotted in (b) (black curve) along with the PL spectra of QD2 taken in  $\sigma+$  polarization.

Looking at the  $\sigma$  polarized emission of this state (Fig. I.8(b) and (c)), we can see that this excitation presents a really good spin conservation: the low and high energy peaks are strongly  $\sigma$  polarized, while the central peaks do not show dependency over circular polarization. This, once again, show the good spin conservation of the system, as highlighted on the quasi-resonant state.

Finally, another interesting excited state appear at 2030 meV. This state presents an exchange-induced splitting different from the splitting in the quasi-resonant state. This is due to a difference in the carriers and Cr atom wavefunction overlap. One can also noticed the this state presents a stronger luminescence in  $\sigma_{cross}$  than in  $\sigma_{co}$ , [TO REDISCUSS] hinting at a spin flip of the hole before the recombination.

### I.1.3 Magneto-optics of a quantum dot doped with a single Cr

The structure of the energy levels in Cr-doped QDs is confirmed by the evolution of the PL spectra in magnetic field (up to 11T) in Faraday configuration [8], presented

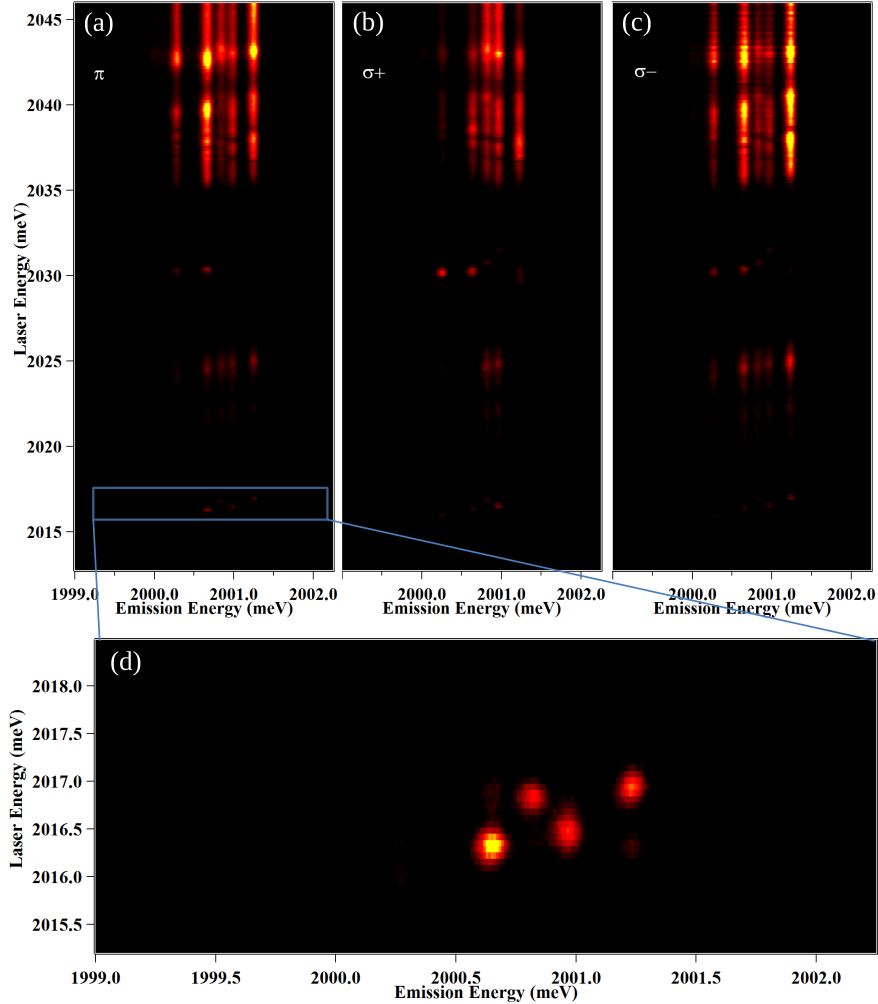


Figure I.8: (a) - (c) PLE map between 2046 meV and 2013 meV presenting several excited, detecting in  $\pi$  (a),  $\sigma+$  (b) and  $\sigma-$  (c). (d) Zoom in a particular excited state presented a splitting inversion, taken in  $\pi$  detection.

in Fig. I.9. One can see that the Zeeman energy of the exciton under magnetic field can compensate the exciton splitting induced by the exchange interaction with the Cr [9]. For QD3, this results in an anti-crossing of  $|+1\rangle$  and  $| -1\rangle$  excitons due to the e-h exchange interaction around  $B_z=6$  T observed both in  $\sigma+$  and  $\sigma-$  polarizations (anti-crossing (2) and (3) in Fig. I.9(a)).

The low energy emission presented as a dark exciton in Fig. I.4 shows an anti-crossing with the bright excitons under  $B_z$  in  $\sigma-$  polarization (anti-crossing (4) in Fig. I.9). As illustrated in Fig. I.11(b), this anti-crossing arises from a mixing of

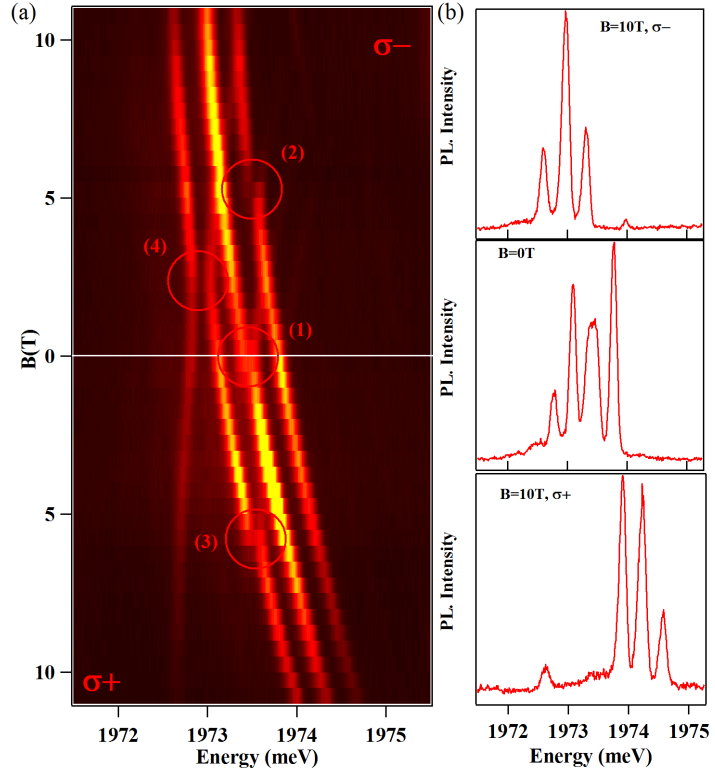


Figure I.9: (a) Circularly polarized X-Cr PL evolution under magnetic field ( $B_z$ ) in QD3. Noticeable anti-crossing are highlighted and numbered. (b) QD3 X-Cr PL spectra taken at 0 and  $\pm 10\text{T}$ .

the bright and dark excitons interacting with the same Cr spin state. Observed in  $\sigma$ - polarization, it corresponds to the mixing of the exciton states  $| -1 \rangle$  and  $| +2 \rangle$  coupled to the Cr spin  $S_z = -1$ . This dark/bright excitons coupling  $\delta_{12}$  is induced by the e-h exchange interaction in a confining potential of reduced symmetry (lower than  $C_{2v}$ ) [10]. In such symmetry, the dark exciton acquire an in-plane dipole moment which lead to possible optical recombination at zero magnetic field [6] as observed in these QDs. The oscillator strength of this "dark exciton" increases as the initial splitting between  $| -1 \rangle$  and  $| +2 \rangle$  excitons is reduced by the magnetic field (Fig. I.11(b)).

To illustrate the influence of the QD symmetry on the magneto-optical properties of X-Cr, we show in Fig. I.10(b) the emission of a QD with a different strain state (QD4). For QD3, the splitting of the central peak is not clear in the PL at 0T (Fig. I.1(a)) without the linear polarization map, while two linearly polarized peaks appears clearly in QD4 spectra. This difference in emission arise from a

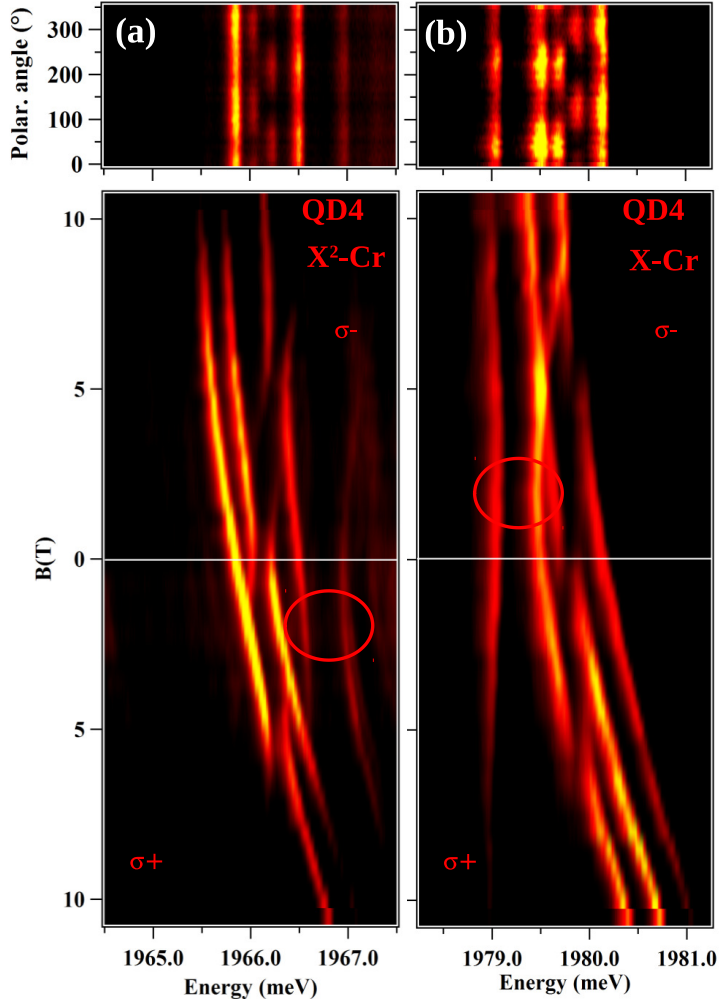


Figure I.10: Linear polarization intensity map (top panel) and intensity map of the longitudinal magnetic field dependence of the emission (bottom panel) of (a)  $X^2\text{-Cr}$  and (b)  $X\text{-Cr}$  in QD4.

difference in the in-plane strain of each QD [4]. The dark exciton emission is also stronger in QD2, confirming a lower symmetry than QD3.

Investigating both the biexciton and the exciton in the same Cr-doped QD, we can also analyze the impact of the carrier-Cr interaction on the fine structure of the Cr spin. The magnetic field dependency of  $X^2\text{-Cr}$  emission in QD2 is presented along with the  $X\text{-Cr}$  emission as a contour plot in Fig. I.10(a) and (b) respectively. The PL under magnetic field of  $X\text{-Cr}$  and  $X^2\text{-Cr}$  present a mirror symmetry. In

particular, the dark/bright exciton mixing observed around  $B_z=2.5\text{T}$  on the low energy side of the PL in  $\sigma-$  polarization for X-Cr is observed on the high energy side in  $\sigma+$  polarization for  $\text{X}^2\text{-Cr}$  (circles in Fig. I.10(a) and (b)).

If one consider the ground state of  $\text{X}^2$  as a spin-singlet (total spin 0), it cannot be split by the magnetic field or the spin interaction part of the carriers-Cr Hamiltonian. The creation of two excitons in the QD cancels the exchange interaction with the Cr atom. Thus, the PL of  $\text{X}^2\text{-Cr}$  is controlled by the final state of the optical transitions, i.e. the eigenstates of X-Cr, resulting in the observed mirror symmetry in the PL spectra. However, in some of the QDs, the  $\text{X}^2\text{-Cr}$  emission slightly deviates from this simple picture: a smaller energy splitting is observed for  $\text{X}^2\text{-Cr}$  compared to X-Cr (see X-Cr and  $\text{X}^2\text{-Cr}$  in Fig. I.10). This shows that there is an interaction of  $\text{X}^2$  with the Cr atom. It could result from a perturbation of the carriers' wave function by the interaction with the magnetic atom [11, 12] or a modification the local electric field which controls the Cr fine structure. [TO BE INVESTIGATED]

## I.2 Modelization of a Cr-doped QD

We calculated the magneto-optic behaviour of Cr-doped QDs by diagonalizing the complete Hamiltonian of the e-h-Cr in self-assembled dots. This hamiltonian can be separated as follows:

$$\mathcal{H}_{X-Cr} = \mathcal{H}_{Cr,\varepsilon} + \mathcal{H}_{c-Cr} + \mathcal{H}_{mag} + \mathcal{H}_{e-h} + \mathcal{H}_{band} + \mathcal{H}_{scat} \quad (\text{I.2})$$

where:

$\mathcal{H}_{Cr,\varepsilon}$  describes the fine structure of the Cr atom and its dependency on local strain, as presented in Eq. ???. It is mainly driven by  $D_0$ , the magnetic anisotropy.  $E$ , the in-plane strains, also appears in this Hamiltonian, but have to be kept small in order to model the found dots (see Fig. I.12 for the emission of a dot with a higher  $E$ ).

$\mathcal{H}_{c-Cr}$  describes the coupling of the electron and hole with the Cr spin, depending on  $I_{eCr}$ , the exchange integral of the electron-Cr spins, and  $I_{hCr}$ , the exchange integral of the hole-Cr spins, as described in Eq. ??.

$\mathcal{H}_{mag}$  describes the effect of an exterior magnetic field, coupled to both the Cr and carrier spins by the Zeeman terms, depending on the  $g$ -factor of each of them, and including the diamagnetic shift of the electron-hole via the term  $\gamma$ .

$$\mathcal{H}_{mag} = g_{Cr}\mu_B \vec{B} \cdot \vec{S} + g_e\mu_B \vec{B} \cdot \vec{\sigma} + g_h\mu_B \vec{B} \cdot \vec{J} + \gamma B^2 \quad (\text{I.3})$$

$\mathcal{H}_{e-h}$  describes the short range and long range electron-hole interaction, through the bright and dark exciton splitting  $\delta_0$ , the bright exciton coupling  $\delta_1$ , the dark

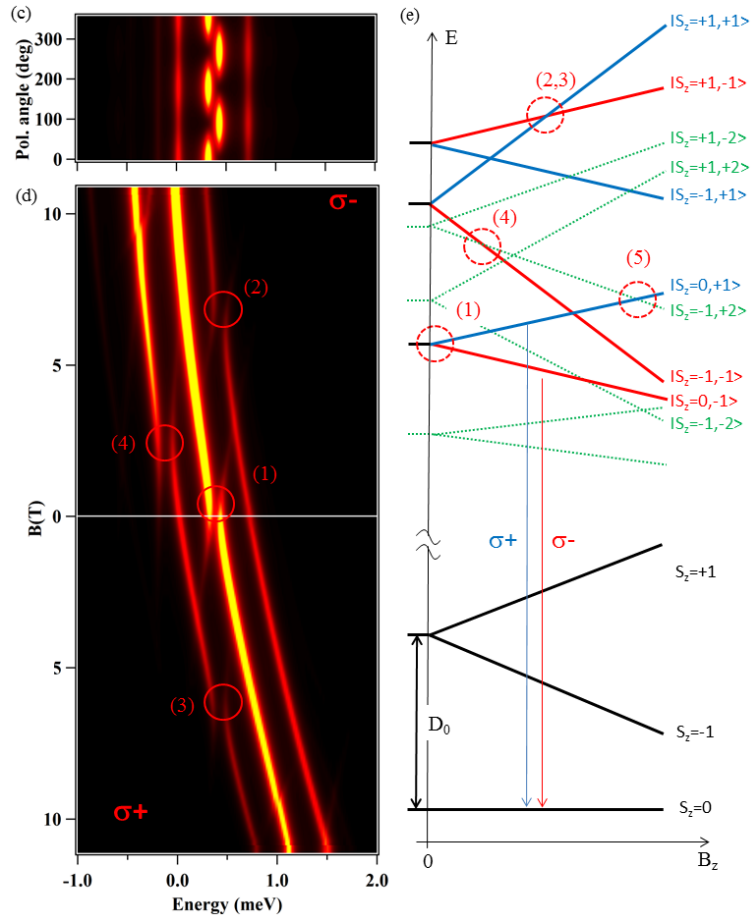


Figure I.11: (a) Up: Calculated linear polarization PL intensity map of X-Cr at zero field. The  $0^\circ$  polarization angle correspond to an emission polarized along the 100 axis. Down: Calculated X-Cr circularly polarized magnetic field dependency. Details of the model and parameters are listed in Tab. I.1. Corresponding anti-crossing are highlighted in same fashion as on Fig. I.9. (b) Schema of the magnetic field dependency of the energy levels of the low energy Cr spin states  $S_z=0$  and  $S_z=\pm 1$ , and corresponding bright ( $|+1\rangle$  blue,  $| -1 \rangle$  red) and dark ( $|\pm 2\rangle$  green) X-Cr energy levels.

exciton coupling  $\delta_2$  and the bright and dark exciton coupling  $\delta_{11}$  and  $\delta_{12}$ . All of these term are described in Eq ??.

$\mathcal{H}_{band}$ , the band Hamiltonian, presented in Eq. ??, stands for the energy of the electrons (i.e. the band gap energy  $E_g$ ), and the heavy-holes (hh) and light-holes (lh) energies, depending on the splitting between lh and hh  $\Delta_{lh}$ , and the anisotropy

Table I.1: Values of the parameters used in the model of Cr-doped CdTe/ZnTe quantum dot presented in Fig. I.11. The value of the parameters not listed in the table is 0. The chosen values are typical for CdTe/ZnTe quantum dots and can be compared with parameters extracted from Mn-doped quantum dots [13, 14]. These values are reasonable to reproduce the emission of the QDs presented in this thesis.

$I_{eCr}$	$I_{hCr}$	$\delta_0$	$\delta_1$	$\delta_{12}$	$\delta_{11}$	$\frac{ Q }{\Delta_{lh}}$	$\frac{ R }{\Delta_{lh}}$
$\mu eV$	$\mu eV$	$meV$	$\mu eV$	$\mu eV$	$\mu eV$		
-70	-280	-1	250	150	50	0.05	0.05
$\arg(R)$	$D_0$	$g_{Cr}$	$g_e$	$g_h$	$\gamma$	$\eta$	$T_{eff}$
	$meV$				$\mu eV/T^2$	$\mu eV$	K
$-\frac{\pi}{2}$	2.5	2	-0.7	0.4	1.5	25	25

of the QD.

$\mathcal{H}_{scat}$  describes the perturbation of the wave function of the exciton in the initial state of the optical transition by the hole-Cr exchange interaction, controlled by the parameter  $\eta$ . This perturbation depends on the value of the exchange energy between the Cr spin  $S_z$  and the hole spin  $J_z$  and can be represented, using second order perturbation theory, by an effective spin Hamiltonian [11, 12, 13]

$$\mathcal{H}_{scat} = -\eta S_z^2 \quad (\text{I.4})$$

with  $\eta > 0$ .

We considered the general case of QDs with a symmetry lower than  $C_{2v}$  (truncated ellipsoidal lens for instance [10]), and took into account the influence of this reduced symmetry on the valence band and on the e-h exchange interaction. The population of the X-Cr spin states split by the large magnetic anisotropy and the carriers-Cr exchange interaction is described by a spin effective temperature  $T_{eff}$ . The results of the model obtained with  $T_{eff}=25\text{K}$ ,  $D_0=2.5\text{ meV}$  and an electron-Cr (hole-Cr) exchange interaction  $I_{eCr}=-70\mu eV$  ( $I_{hCr}=-280\mu eV$ ) are reported in Fig. I.11 (parameters not specific to Cr-doped QDs are listed in Tab. I.1). Such parameters do not aim to fit the data and are only reasonable order of magnitude. The PL of X-Cr at zero field and its evolution in magnetic field can be qualitatively reproduced. In particular, the description of the spin states occupation by  $T_{eff}$  is sufficient to reproduce the observed emission from the three low energy X-Cr levels (Cr spin states  $S_z=0$  and  $S_z=\pm 1$ ). The splitting of the central line at zero field (anti-crossing (1)) and the anti-crossings under magnetic field (anti-crossings (2) and (3) around  $B_z=6\text{T}$  for the Cr spin states  $S_z=+1$  and anti-crossings (4) with the dark exciton around  $B_z=2\text{T}$ ) are also well reproduced by the model.

The magnetic anisotropy  $D_0$  cannot be precisely extracted from the PL spectra.

However, a higher value would produce a smaller PL intensity of the states  $S_z=|\pm 1\rangle$  than observed experimentally. In addition, for  $D_0 < 2.25$  meV, an anti-crossing due to an electron-Cr flip-flop controlled by  $I_{eCr}$ , labelled (5) in Fig. I.11(c), would appear below  $B_z=11$ T on the central line in  $\sigma+$  polarization.

Having shown that our model reproduce well the evolution of the emission under variations of different parameters, we can run it to see the influence of  $E$  on the emission. This simulation was done by applying a small magnetic anisotropy  $D_x$  along the  $x$  axis of the quantum dot and none along the  $y$  axis ( $D_y=0$ ), creating an effective  $E$ . Results of such a study are presented on Fig. I.12, (a) and (b) for the X-Cr system, and (c) and (d) for the  $X^c$ -Cr one.

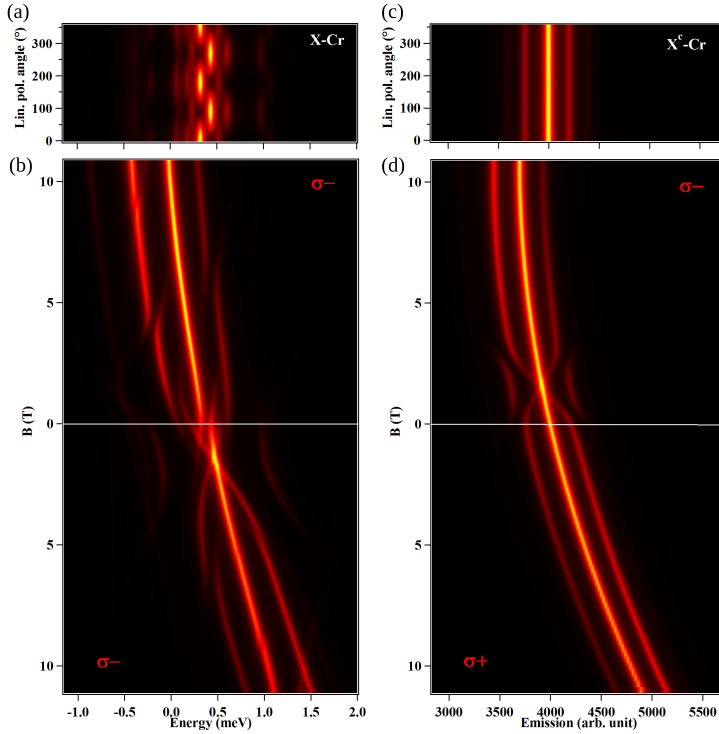


Figure I.12: For a QD with a small magnetic anisotropy along the  $x$  axis ( $D_x = 150 \mu\text{eV}$ ,  $D_y = 0 \mu\text{eV}$ ,  $D_z = 2500 \mu\text{eV}$ ): (a) calculated X-Cr linear polarization PL intensity at 0T; (b) calculated X-Cr circularly polarized magnetic field dependency; (c) calculated  $X^c$ -Cr linear polarization PL intensity at 0T; and (d) calculated  $X^c$ -Cr circularly polarized magnetic field dependency.

The X-Cr map in linear polarization presents a dependency on all the three peaks at 0T, when only the central peaks exhibit this behaviour in dots with a small in-plane anisotropy at the Cr position. The effect of such an anisotropy

is to couple to spin levels separated by two spin units, such as  $|S_z = -1\rangle$  and  $|S_z = +1\rangle$ . This induces a mixing between two bright exciton states, leading to a linearly polarized emission. For a low E value, the strain induced splitting of  $|S_z = \pm 1\rangle$  is high enough to strongly reduce the mixing of the exciton states. A higher in-plane strain anisotropy is able to couple the spin level and induce the linearly polarized emission.

As can be expected, X<sup>c</sup>-Cr doesn't present any linear polarization dependency, as shown on Fig. I.12(c).

The evolution of the emission under magnetic field also presents different characteristics than a QD with magnetic anisotropy purely along z. Fig. I.12(b) presents the evolution in B of the X-Cr emission. One can note anti-crossings at +5T appearing on both  $|S_z = +1\rangle$  and  $|S_z = -1\rangle$ , as well as an anti-crossing at -5T appearing on the low energy emission lines. These are similar to the anti-crossing (2), (3) and (4) on Fig. I.11. Around 0T, other anti-crossings appear, on all the three peaks this time. Anti-crossing on the central peaks is the same as the anti-crossing (1) in Fig. I.11. The ones appearing on the  $|S_z = \pm 1\rangle$  peaks arise from the exciton mixing via E, as evidenced by the linear polarization.

X<sup>c</sup>-Cr in dot with high in-plane anisotropy at the Cr position also presents anti-crossing for a magnetic field around 1T, as shown in Fig. I.12(d). This anti-crossing appears when the Zeeman effect of the Cr atom compensates the electron-Chromium interaction and the hole-Chromium interaction.

### I.3 The case of six peaks dots

Some dots were found presenting a linear polarization dependency both on their central peaks and on their exterior peaks. However, such dots didn't present any anti-crossing when probed under magnetic field. Results of these experiments are presented in Fig. I.13.

A common feature of all of these dots is the thin and well split X<sup>+</sup>-Cr PL structure, shown on Fig. I.13(a) around 1949mev. X-Cr and X<sup>2</sup>-Cr also present three well defined peaks, with a broad emission. This is not a general case, as some dots were found presenting a broad emission on X-Cr and X<sup>2</sup>-Cr positions, such as QD6 presented in Fig. I.15. The linear polarization map of the PL of QD4 reveals that each peak presents a linear polarization dependency (Fig. I.13(b) and (c)).

The PL evolution of such a dot is presented in Fig. I.13(d). The diamagnetic shift is clearly visible. However, the only anti-crossings appear at B=9T for all the peaks (zoom in Fig. I.13(d)). Such anti-crossings are characteristic of an exciton in a QD with no magnetic atom: it arises from the dark and bright exciton mixing.

In order to get more informations on these dots, it was decided to study them

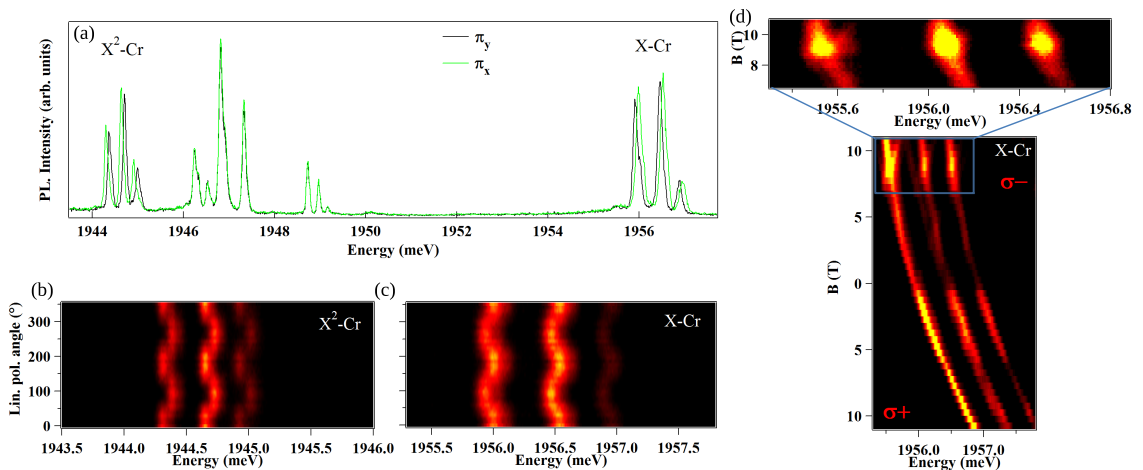


Figure I.13: (a) QD4 linearly polarized PL intensity at zero magnetic field. (b) and (c) Respectively X<sup>2</sup>-Cr and X-Cr linear polarization PL dependence at zero magnetic of this QD. Both central and exterior peaks present linear polarization dependencies in this dots. (c) X-Cr magnetic field PL dependence on this QD. Zoom in presents anti-crossing appearing at B=9T.

applying a bias voltage. The application of an electric field was realized via a sample with a Schottky gate in the same fashion than the one in chap. ???. The resulting map is presented in Fig. I.14(a). The first visible feature is the strong electric field dependency of the emission energy, more marked for X-Cr than for the X<sup>c</sup>-Cr systems. The emission energy variation of the X-Cr complex occur on a 2.9 meV scale.

There is another remarkable point on these maps, evidenced on the X<sup>+</sup>-Cr complex on the Fig. I.14(b): the splitting between each peak is changing with the applied electric field. The splitting between the high and low energy peaks varies from 0 meV for an applied bias voltage of -12V (no splitting) to 0.76 meV for 13V applied. This disappearance of the splitting for a certain bias voltage indicates that the overlap between the electron and the hole wave functions is changed by the application of an exterior electric field, to the point where they don't overlap at all.

Fig. I.15 shows that, using electric field, we can manipulate the splitting of any given charged state of the QD. For all positive bias voltage between 0V and 13V, X-Cr present a broad emission containing all six peaks in linear emission, as show on Fig. I.15(a). The emission then divide into three distinct peaks, starting to appear around -1V. This is evidenced on the the PL emission on Fig. I.15(d).

This three peaks emission structure looks like a three levels system emitting

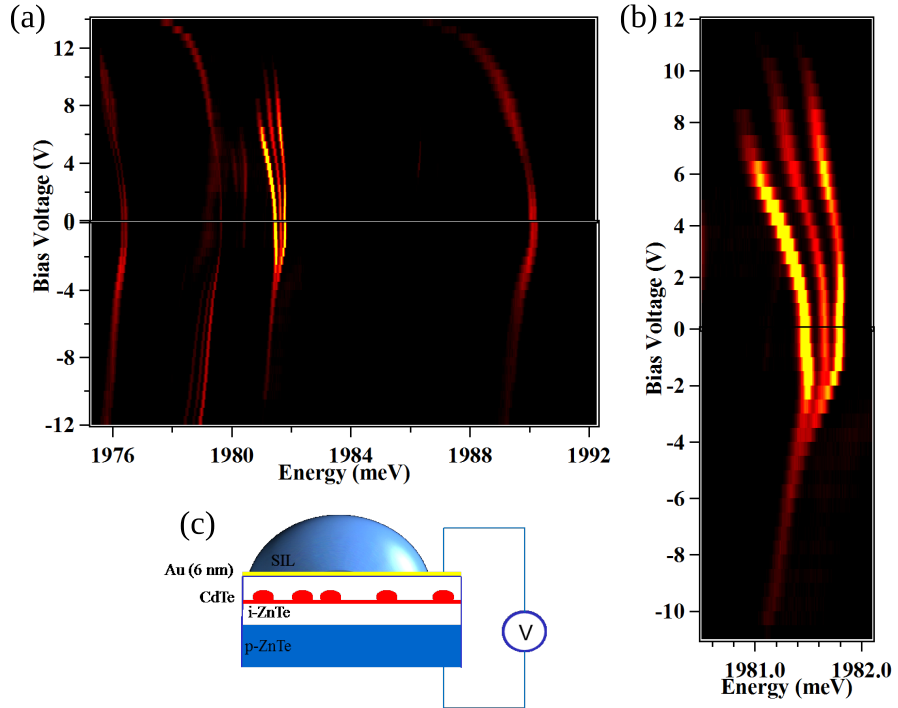


Figure I.14: (a) QD5 whole PL evolution under application of a bias voltage. (b) Zoom on  $X^c$ -Cr circular polarization PL intensity evolution under electric field. A strong stark shift is observed, as well as variation in the splitting. (c) Schema of the Schottky gate used to apply the bias voltage on the sample.

at three different energies. However, the magnetic field evolution presented in Fig. I.13(c) does not reflect the presence of a magnetic atom in the quantum dot. Moreover, evolution under electric field shows huge changes in the carriers wave functions overlap. These features hint for a single exciton trapped in the QD, presenting spectral fluctuations.

Spectral fluctuations under a fluctuation of charge in the vicinity of a QD has been observed to lead to a peak broadening [15], such as observed on Fig. I.15(d), as well as spectrum jumps. For the PL to jump between three emission energies, the charge fluctuation has to be able to take three distinct charge values.

Cr in ZnTe is incorporated as  $\text{Cr}^{2+}$ , but, as shown on Fig. I.16(a), the  $\text{Cr}^+$  and  $\text{Cr}^{3+}$  are also accessible [16], either by capturing an electron ( $\text{Cr}^+$ ) or a hole ( $\text{Cr}^{3+}$ ). Considering such a charge close to the QD, it can be viewed as a punctual one, since the dot is far bigger than the atom. The effect on the wave functions, presented in Fig. I.16(b)-(d), differs depending on the electrical charge of the Cr

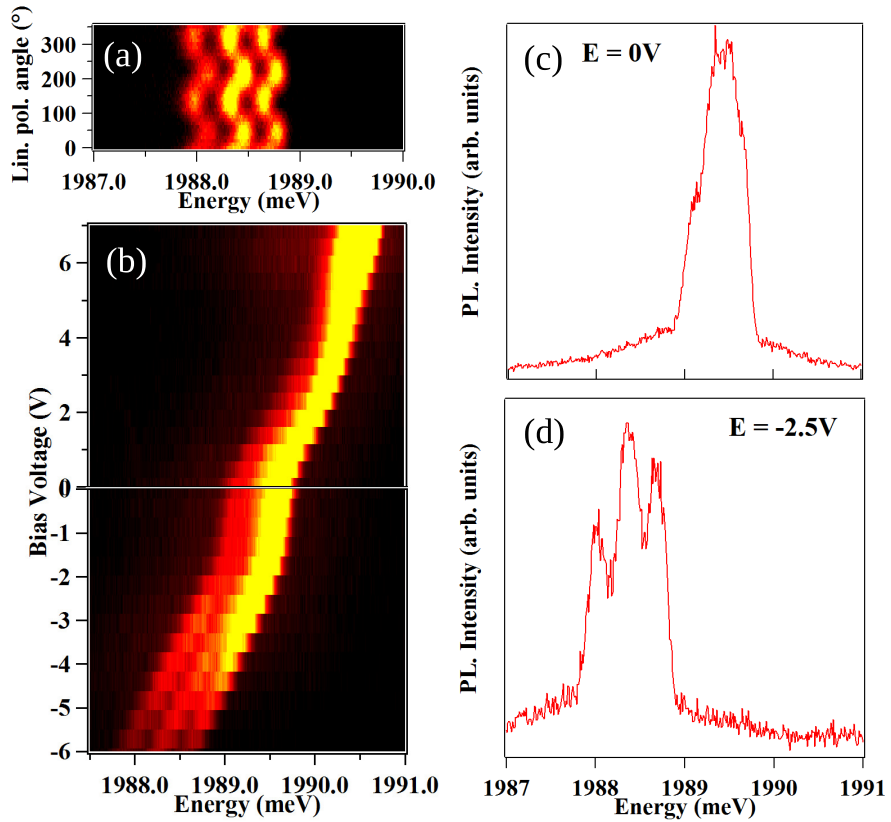


Figure I.15: All these measures were taken on QD6 X-Cr complex at low temperature. (a) PL intensity dependency in linear polarization. In order to have the best contrast, the map was taken at -2.5V bias voltage. (b) Circular PL intensity evolution in electric field. A splitting began to appear around -2V of applied bias voltage. (c)-(d) Circular PL for an applied bias voltage of, respectively, 0V and -2.5V.

atom. The electron is well confined in CdTe/ZnTe quantum dots, while the hole is almost not confined. Because of this, the electron wave function is almost not moved by the presence of the electric, when the hole one vary more depending on the charge state of the Cr. These differences in the overlapping of wave functions lead to three different emission energies depending on the Cr charge state.

The charge variation of the Cr is of the value of the elementary charge. Considering a pure coulomb interaction between two punctual charges, for a charge at 5nm of the dot, its effect is one order of magnitude below the confinement energy. In order to have a significant effect on the dot PL, the Cr has then to be close to it, not more than a few nanometres away.

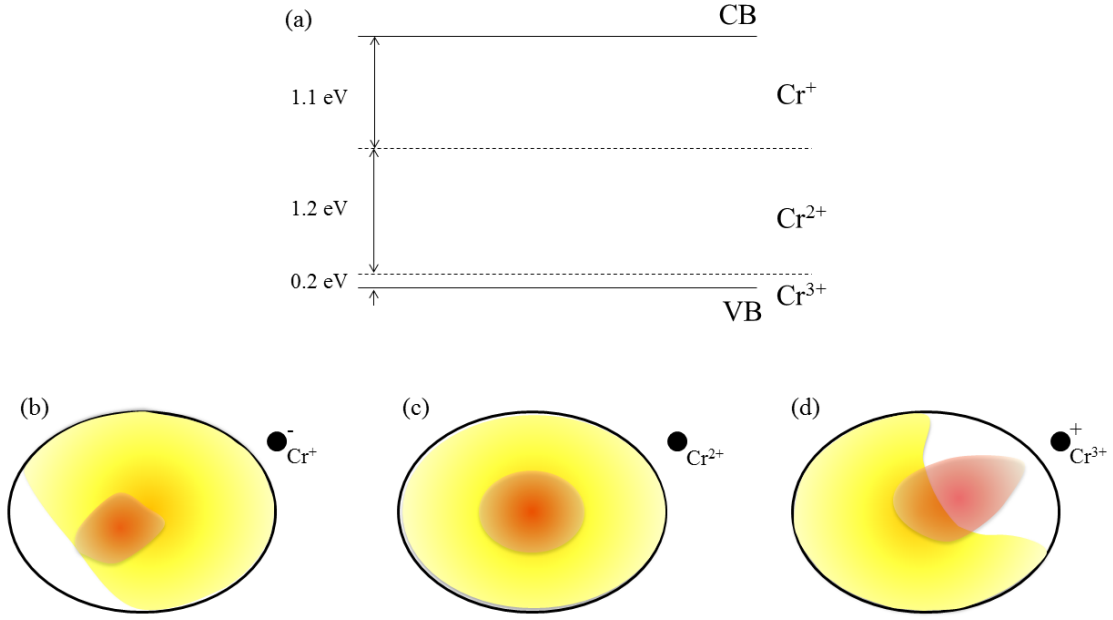


Figure I.16: (a) Cr accessible charged states in ZnTe. (b)-(d) Illustration of the effect of a punctual charge on the wavefunction of an electron (red) and a hole (yellow) in a quantum dots.

This hypothesis is currently tested, along with the capacity for the Cr to diffuse outside the quantum dots layer.

## I.4 Conclusion

For the first time, a single Cr atom in a semiconductor was probed optically. The fine structure of the Cr is dominated by a magnetic anisotropy induced by strain in the plane of the QDs. The large spin to strain coupling of Cr, two orders of magnitude larger than for magnetic elements without orbital momentum (NV centers in diamond [17], Mn atoms in II-VI semiconductors [18]) suggests some possible development of coherent mechanical spin-driving of an individual magnetic atom in a nano-mechanical oscillator. This new single spin system should allow, at low temperature, to enter some coupling regimes dominated by quantum coherent dynamics not reached until now in hybrid spin-mechanical devices.

# Chapter II

## Bibliography

- [1] J. T. Vallin and G. D. Watkins. Epr of cr<sup>2+</sup> in II-VI lattices. *Phys. Rev. B*, 9:2051–2072, Mar 1974.
- [2] W. Mac, A. Twardowski, and M. Demianiuk. s,p-d exchange interaction in Cr-based diluted magnetic semiconductors. *Phys. Rev. B*, 54:5528–5535, Aug 1996.
- [3] M. Herbich, W. Mac, A. Twardowski, K. Ando, Y. Shapira, and M. Demianiuk. Magnetization and exciton spectroscopy of the diluted magnetic semiconductor cd<sub>1-x</sub>cr<sub>x</sub>S. *Phys. Rev. B*, 58:1912–1921, Jul 1998.
- [4] T. Takagahara. Theory of exciton doublet structures and polarization relaxation in single quantum dots. *Phys. Rev. B*, 62:16840–16855, Dec 2000.
- [5] J. McFarlane, P. A. Dalgarno, B. D. Gerardot, R. H. Hadfield, R. J. Warburton, K. Karrai, A. Badolato, and P. M. Petroff. Gigahertz bandwidth electrical control over a dark exciton-based memory bit in a single quantum dot. *Applied Physics Letters*, 94(9):093113, 2009.
- [6] M. Bayer, G. Ortner, O. Stern, A. Kuther, A. A. Gorbunov, A. Forchel, P. Hawrylak, S. Fafard, K. Hinzer, T. L. Reinecke, S. N. Walck, J. P. Reithmaier, F. Klopf, and F. Schäfer. Fine structure of neutral and charged excitons in self-assembled in(ga)as//(al)gaas quantum dots. *Phys. Rev. B*, 65:195315, May 2002.
- [7] D. Gammon, E. S. Snow, B. V. Shanabrook, D. S. Katzer, and D. Park. Fine structure splitting in the optical spectra of single GaAs quantum dots. *Phys. Rev. Lett.*, 76:3005–3008, Apr 1996.
- [8] L. Besombes and H. Boukari. Resonant optical pumping of a Mn spin in a strain-free quantum dot. *Phys. Rev. B*, 89:085315, Feb 2014.

- [9] Y. Léger, L. Besombes, L. Maingault, D. Ferrand, and H. Mariette. Geometrical effects on the optical properties of quantum dots doped with a single magnetic atom. *Phys. Rev. Lett.*, 95:047403, Jul 2005.
- [10] M. Zieliński, Y. Don, and D. Gershoni. Atomistic theory of dark excitons in self-assembled quantum dots of reduced symmetry. *Phys. Rev. B*, 91:085403, Feb 2015.
- [11] L. Besombes, Y. Leger, L. Maingault, D. Ferrand, H. Mariette, and J. Cibert. Carrier-induced spin splitting of an individual magnetic atom embedded in a quantum dot. *Phys. Rev. B*, 71:161307, Apr 2005.
- [12] Anna H. Trojnar, Marek Korkusinski, Udsion C. Mendes, Mateusz Goryca, Maciej Koperski, Tomasz Smolenski, Piotr Kossacki, Piotr Wojnar, and Paweł Hawrylak. Fine structure of a biexciton in a single quantum dot with a magnetic impurity. *Phys. Rev. B*, 87:205311, May 2013.
- [13] B. Varghese, H. Boukari, and L. Besombes. Dynamics of a Mn spin coupled to a single hole confined in a quantum dot. *Phys. Rev. B*, 90:115307, Sep 2014.
- [14] Y. Léger, L. Besombes, L. Maingault, and H. Mariette. Valence-band mixing in neutral, charged, and Mn-doped self-assembled quantum dots. *Phys. Rev. B*, 76:045331, Jul 2007.
- [15] H. Kamada and T. Kutsuwa. Broadening of single quantum dot exciton luminescence spectra due to interaction with randomly fluctuating environmental charges. *Phys. Rev. B*, 78:155324, Oct 2008.
- [16] Dziesiaty J., Peka P., Lehr M. U., Klimakow A., Müller S., and Schulz H.-J. The chromium impurity in znte: Changes of the charge state detected by optical and epr spectroscopy. *ZPCH*, 201:63, Jan 1997.
- [17] A. Barfuss, J. Teissier, E. Neu, A. Nunnenkamp, and P. Maletinsky. Strong mechanical driving of a single electron spin. *Nat Phys*, 11:820, Oct 2015.
- [18] A. Lafuente-Sampietro, H. Boukari, and L. Besombes. Strain-induced coherent dynamics of coupled carriers and Mn spins in a quantum dot. *Phys. Rev. B*, 92:081305, Aug 2015.